Strong Purcell Effect on a Neutral Atom Trapped in an Open Fiber Cavity

J. Gallego,[*] W. Alt, T. Macha, M. Martinez-Dorantes, D. Pandey, and D. Meschede

Institut für Angewandte Physik der Universität Bonn, Wegelerstrasse 8, D-53115 Bonn, Germany

We observe a sixfold Purcell broadening of the D_2 line of an optically trapped ^{87}Rb atom strongly coupled to a fiber cavity. Under external illumination by a near-resonant laser, up to 90% of the atom's fluorescence is emitted into the resonant cavity mode. The sub-Poissonian statistics of the cavity output and the Purcell enhancement of the atomic decay rate are confirmed by the observation of a strongly narrowed antibunching dip in the photon autocorrelation function. The photon leakage through the higher-transmission mirror of the single-sided resonator is the dominant contribution to the field decay ($\kappa \approx 2\pi \times 50$ MHz), thus offering a high-bandwidth, fiber-coupled channel for photonic interfaces such as quantum memories and single-photon sources.

The modification of the photoemission properties of matter is a field of broad and current interest in the pursuit of controlled and efficient light-matter interfaces. The use of a resonator to enhance the spontaneous emission rate of an atom was proposed by E. M. Purcell [1] and later observed in the microwave [2] and optical domains [3]. According to his proposal, in the presence of a cavity with a single resonant field mode, the decay rate (2γ) of an excited atom is enhanced by the factor f_P, which in cavity quantum electrodynamics (CQED) is related to the cooperativity of the system by $f_P = 2C = g^2/(\kappa\gamma)$. Here, g is the atom-field interaction strength, and κ stands for the decay rate of the cavity field. Notably, the directionality of the atomic emission is also enhanced, and the cavity mode collects a fraction of the photons given by $f_P/(f_P + 1)$. Both effects facilitate the generation and efficient collection of single photons, and thus, the study of the Purcell effect has been extended to multiple types of emitters. These include atoms [4,5], quantum dots [6,7], and a variety of other solid-state systems [8–11] amongst others, with particular emphasis on the development of single-photon sources (SPS) [12–18]. The required high cooperativities can be obtained by tailoring the resonator, i.e., reducing the mirror transmission and losses (for low κ), or the mode volume (for high g). However, to build an efficient SPS with a high-rate output, the resonator must supply a photon out-coupling rate faster than the spontaneous emission rate, i.e., $\kappa \gg \gamma$. A strong Purcell enhancement in such *open*-cavity platforms can only be realized by using microresonators with reduced mode volume [19] or emitters with narrow emission lines, like neutral atoms and ions [20–23]. Large Purcell factors have been recently realized for narrow forbidden lines of Er^{3+} ions in solid-state hosts [11]. However, these solid-state systems are still not within the desired regime of $g > \kappa \gg \gamma$, where the dominant

coherent interaction allows for the reversible storage of quantum information, of particular interest for the creation of efficient hybrid quantum communication links.

Atom-based platforms guarantee highly controllable, coherent, and reproducible photon sources, without the need for cryogenic equipment. Of particular interest is their integration with fiber Fabry-Pérot cavities (FFPCs) [24], which can host mode volumes of the order of the emission wavelength λ^3 [25] while offering high tunability, intrinsic fiber coupling, and a good radial optical access, which is critical for the external manipulation of the emitter. The rapid progress seen in FFPC platforms in recent years [26–29] includes the demonstration of Purcell broadening on the photoemission of atoms [4,5,30]; however, in all reported cases, single-atom Purcell factors remained well below unity. Substantial cooperativities have only been shown for transient dense clouds of atoms [4], extremely *closed* macroscopic cavities ($\kappa \approx \gamma$) [12,16], or in a setup without external addressing [20]—all of those scenarios preventing its use as a high-bandwidth SPS. In this Letter, we demonstrate the highest Purcell broadening so far directly observed for an externally driven, single atom. Our system consists of a neutral ^{87}Rb atom optically trapped inside an open FFPC. We show that the platform operates in the desired open cavity regime, with an emission spectrum displaying a line broadening corresponding to $f_P \approx 5$, a factor that increases up to 20 when pumping the atom better towards the strongest transition. The homogeneous nature of the broadening is confirmed by analyzing the output of the cavity with a Hanbury Brown–Twiss setup, which reveals a narrow antibunching dip corresponding to the generation of single photons from an atom with a strongly shortened lifetime.

The core of our experimental apparatus is a one-sided high-finesse FFPC (described in detail in [31]) where one
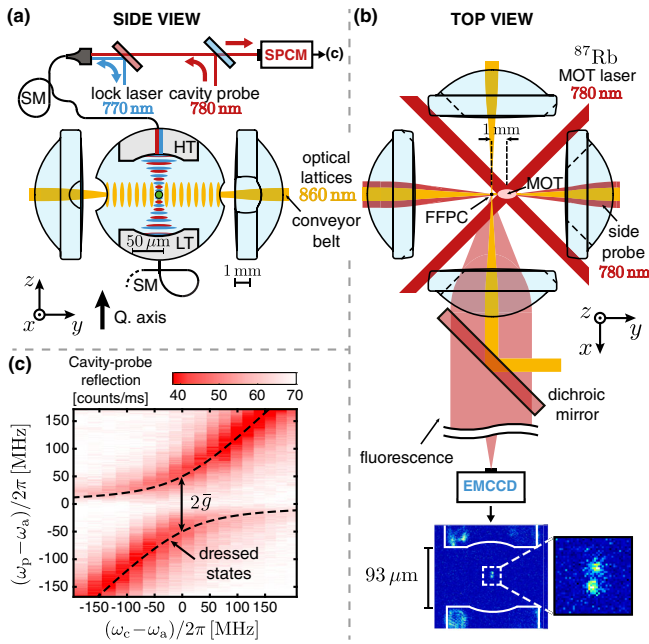
FIG. 1. Experimental setup. (a) Side- and (b) top-view technical drawing of the main components and the relevant light fields, showing the cavity- and side-probe configurations, respectively. The bottom inset shows a fluorescence image of two atoms coupled to the resonator (20 ms exposure time). (c) Probe power reflected from the cavity ($\kappa = 2\pi \times 58$ MHz), showing the energy bands of the coupled atom-cavity system for a weakly-pumped single atom. The dashed lines display the dressed states of the addressed cycling transition ($|F, m_F\rangle = |2, 2\rangle \leftrightarrow |3', 3'\rangle$). For each cavity frequency (ω_c), the probe frequency ω_p is scanned through resonance.

of the fiber mirrors features a relatively high transmission (HT), thus serving as an efficient input-output coupling channel. The coating characteristics and the length of the resonator lead to an initial field decay rate of $\kappa \approx 2\pi \times 25$ MHz, which later degraded under vacuum conditions (see Supplemental Material [32]). The cavity is placed at the center of an integrated, compact mount featuring four aspheric lenses with high numerical apertures (NA = 0.5, see Fig. 1), which are the keystone of the high degree of optical control in our system [41]. Amongst other applications, they are used to strongly focus two pairs of counter-propagating, red-detuned dipole-trap beams (860 nm), which create a two-dimensional optical lattice [see Figs. 1(a),(b)]. The "lock laser" (770 nm) employed to stabilize the resonator's length [31] also serves as a blue-detuned intracavity dipole trap, resulting in a three-dimensional (3D) subwavelength confinement of the atom at the antinodes of the cavity mode, resonant with the D_2 line of ^{87}Rb (780 nm).

In a typical experiment, a few tens of neutral ^{87}Rb atoms are trapped from the background gas (10^{-9} mbar) and cooled down to ~ 50 μK by a magneto-optical trap (MOT)

positioned 1 mm away from the cavity center, as depicted in Fig. 1(b). The atoms are subsequently loaded into one of the optical lattices—which act as an optical conveyor belt [42]—and transported into the cavity region. Once inside the resonator, the presence of a coupled atom is detected by its interaction with a near-resonant probe field (780 nm), which is either injected into the cavity or focused on the atom by the in-vacuum lenses [Figs. 1(a) and 1(b), respectively].

In the first case, referred to as the "cavity probe," the presence of an atom manifests as a rise in the reflected probe power when the field and the cavity are resonant with the atom. The resulting increase in counts—detected by a single-photon counter module (SPCM)—is used for real-time feedback to halt the transport mechanism as soon as an atom strongly couples to the cavity mode. This ensures the coupling of a single atom in $\sim 85\%$ of the cases. By scanning both the probe frequency and the cavity resonance, a clear avoided crossing appears between the dressed states of the coupled system, see Fig. 1(c). From the vacuum Rabi splitting, we obtain an average coupling constant of $\bar{g} = 2\pi \times (49.94 \pm 0.12)$ MHz following a Gaussian distribution of width $\sigma_g = 2\pi \times (18.2 \pm 0.2)$ MHz, as a result of different positions of the atom inside the cavity mode. The system's average single-atom cooperativity is thus approximately $\bar{C} \approx 7.2$ (distributed over a range $C \in [2.9, 13.4]$), which demonstrates the high cooperativity of our platform even for bandwidths $\kappa \gg \gamma$. Such a fast coherent interaction is an essential prerequisite for reversible processes required for photon storage and retrieval [43].

For applications such as SPS, the atom must be directly addressed by an external driving field. This is the role of the second type of illumination—depicted in Fig. 1(b) as a "side-probe"—where the atoms are continuously driven by (typically red-detuned) light in a lin$\perp$lin configuration. The resulting polarization gradient provides one-dimensional cooling, and it prevents the formation of intensity standing waves. The in-vacuum lenses enable not only the required strong focusing of the illumination beam, but also the efficient collection of the photons scattered into free space by the atoms. These are imaged onto an electron-multiplying CCD camera that yields high-resolution fluorescence images, critical for the estimation of the position and number of atoms [inset of Fig. 1(b)]. The large fraction of light scattered into the cavity is monitored by the SPCM and, along with the camera counts, it provides the necessary information to characterize the system's photoemission properties. Such a study requires a model for the scattering rates under the external driving of the atom. As described in the Supplemental Material [32], for a continuous driving field of Rabi frequency Ω and frequency ω_p, the rate of photons emitted in free space (R_{f-s}) or into the cavity (R_c) are

$$R_{f-s} = \frac{\Omega^2/(2\gamma)}{1 + \Delta_a^2/\gamma^2} \frac{1}{|1 + 2\tilde{C}|^2} \qquad (1a)$$

$$R_c = \frac{\Omega^2}{\gamma C} \frac{|\tilde{C}|^2}{|1 + 2\tilde{C}|^2}, \qquad (1b)$$

where we have introduced the complex cooperativity parameter (see e.g., [44])

$$\tilde{C} = \frac{g^2}{2(\kappa - i\Delta_c)(\gamma - i\Delta_a)}, \qquad (2)$$

with $\Delta_{c/a} = \omega_p - \omega_{c/a}$. Here ω_c and ω_a correspond to the cavity resonance and the ac Stark shifted frequency of the atomic cycling transition, respectively.

The model assumes that the atom is a weakly driven two-level system. We consider effects due to power saturation of multilevel transitions by comparing the model to numerical simulations based on the master equation formalism. Externally driving the atom with near-resonant lin⊥lin probe light leads to a reduced effective coupling strength g_{eff} due to the addressing of transitions weaker than the strongest one. In this case $\kappa > g_{\text{eff}} \gg \gamma$, and the system enters the *fast-cavity regime* where the resonator's output ($\propto R_c$) corresponds to a broadened Lorentzian curve of half-width $\gamma_c' = (1 + 2C)\gamma$, which is a direct signature of the Purcell-enhanced atomic decay rate. The effect of the resonator becomes evident when comparing the cavity output line shape to that of uncoupled atoms, given by $R_0 := R_{f-s}(g = 0)$. Both emission spectra are measured by loading an atomic ensemble into the cavity region, with $\bar{N}_{\text{at}} = 1.5$ atoms coupling to the resonator on average. The ensemble is illuminated with side-probe light, the frequency of which is scanned through the system's resonance [with $\omega_a = \omega_c$, see Fig. 2(a)]. The resulting scattering rates are estimated from the detected photon counts as described in the Supplemental Material [32].

Figures 2(b),(d) display the free-space emission line shape of the system, estimated from the camera counts. We assume that such a spectrum corresponds exclusively to uncoupled atoms, since the free-space contribution from coupled atoms is negligible given that $R_{f-s}/R_0 = |1 + 2C|^{-2} \approx 1.5\%$ [see inset in Fig. 2(b)]. The resonance follows a Lorentzian curve of half-width $\gamma_{f-s}' \approx 1.65\gamma$ attributed to a combination of power broadening and inhomogeneous ac Stark shifts of the ensemble in the outer regions of the 3D lattice. We can neglect Doppler and collisional broadenings due to the individual, tight confinement of the atoms. On the other hand, the line shape of the cavity output, shown in Figs. 2(c),(e), stems from photons scattered solely by coupled atoms, and corresponds to the Purcell-broadened spectrum of the coupled system. The effect of the cavity on the atomic properties manifests as a clear broadening of $\gamma_c'/\gamma \approx 8.4$ (corresponding to
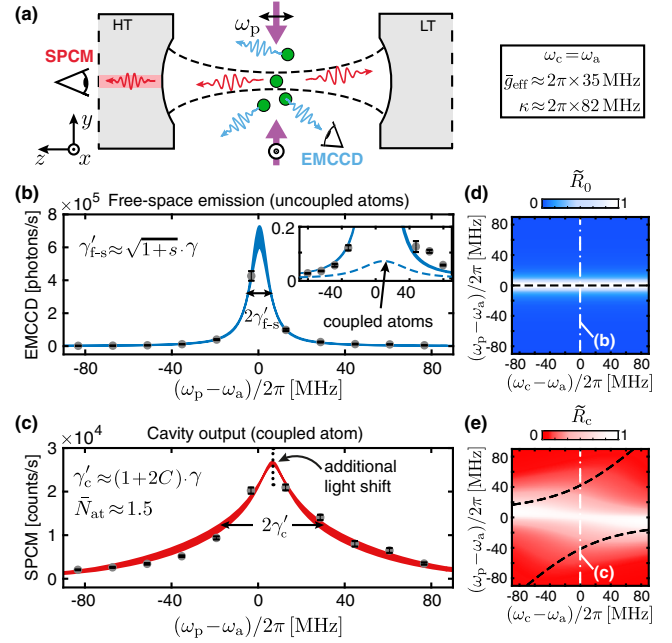

FIG. 2. Purcell-induced broadening of the atomic line shape. (a) Simplified sketch of the measurement for coupled and uncoupled atoms. The lin⊥lin probe light (purple) is scattered either into the cavity mode (red arrows) or into free space (blue arrows). (b) Free-space emission spectrum of atoms trapped outside the cavity mode, error bars indicate the one-sigma statistical error of the mean. The solid line is a fit to a Lorentzian curve, while the dashed line in the inset shows the negligible free-space contribution expected from atoms coupled to the cavity. (c) Emission line shape of the atom-cavity system displaying a clear Purcell broadening. The solid line represents a fit to a convolution of a Lorentzian curve of half-width $\gamma_c' = (1 + g_{\text{eff}}^2/\kappa\gamma)\gamma$ and a Gaussian distribution of coupling strengths with mean $\bar{g}_{\text{eff}}$ and variance σ_g (see main text). Differences in m_F-states population lead to an additional light shift. (d) and (e) are theoretical emission rates for an uncoupled atom in free space ($\tilde{R}_0$, blue) and the cavity output of a coupled system ($\tilde{R}_c$, red, $N_{\text{at}} = 1$) using the fit parameters, both normalized to their maximum value. The dashed, black lines represent the eigenenergies of the system.

$\gamma_c'/\gamma \approx 5.9$ for $N_{\text{at}} = 1$), which yields an average single-atom cooperativity of $\bar{C} = 2.5 \pm 0.3$. We can exclude other effects such as power broadening [as the saturation parameter s scales with $(1 + 2C)^{-2}$] or inhomogeneous light shifts (since the coupled atoms are confined in the well-defined central region of the 3D trap). The difference to the value estimated from Fig. 1 comes from higher mirror losses and a different m_F-level distribution (estimated to lead to $g_{\text{eff}} \approx 0.73\,g$). Such a single-atom cooperativity surpasses by more than an order of magnitude those of similar reported fiber-cavity systems with externally driven atoms [4,5,30], and could be further increased by precise positioning of the atom and a far-detuned driving that addresses stronger transitions (see Supplemental Material [32] for a discussion on the effective coupling strength).

The faster atomic decay inferred from the broadening is also associated to a strong directionality of the photoemission into the cavity mode, given by the ratio

$$R_c/R_{f-s} = \frac{2C}{1 + \Delta_c^2/\kappa^2}, \qquad (3)$$

where the denominator indicates the reduction of the Purcell effect for an off-resonant cavity. Such a directionality is integral to the development of efficient SPS, and its consequences become apparent in our system, due to the continuous driving of the atom inside a high-finesse cavity. In such a scenario, the high fraction of photons scattered into the resonator build up a cavity field that can reach an amplitude comparable to that of the side-probe driving field (or even the same amplitude for $\kappa \to 0$ [45]). The interference between both fields alters the total effective driving experienced by the atom and, therefore, its total scattering rate. The effect depends on the relative phase between both fields, given by the phase shifts acquired from the off-resonant atomic scattering $\propto \Delta_a/\gamma$ and the cavity round-trips $\propto \Delta_c/\kappa$ (see e.g., [5]). Such an effect, dubbed a cavity backaction [5,45–47], is fully contained in the simplified quantum model of Eqs. (1), and confirmed in our experiment by characterizing the photoemission of a single atom coupled to the resonator under red-detuned illumination (see Fig. 3).

Figures 3(b),(d) show how the feedback of the cavity field on the atomic emission leads in general to an enhancement of photon scattering into free space. The curve follows the behavior predicted by Eq. (1), including the detuning conditions that lead to the boundary $R_{f-s} = R_0$ between scattering enhancement and reduction (given by $\Delta_c\Delta_a/(\kappa\gamma) = 1 + C$). Although the emission reduction is not obvious in this particular data set (due to uncertainties in the collection efficiency), clear effects are observed for higher driving powers (see Fig. S.3 in the Supplemental Material [32]). The corresponding cavity emission [shown in Figs. 3(c),(e)] displays a curve with a maximum emission rate 15 times higher than the total emission from an uncoupled atom. The peak corresponds to the probe light being resonant to one of the dressed states of the coupled system, and results from the combination of constructive backaction and Purcell directionality, with an estimated average cooperativity of $\bar{C} = 11.3 \pm 1.0$. This value is superior to that shown in the previous measurement due to a higher cavity finesse, the far-detuned driving, and the pre-selection of strongly coupled atoms by the transport feedback and a push-out technique (see Supplemental Material [32]). The ratio between the rates shown in Figs. 3(c) and 3(b) is given by Eq. (3), and when the resonator and the probe are resonant, a maximum cavity collection efficiency of $\beta \approx 90.4 \pm 1.4\%$ is obtained. Because of the presence of a single quantum emitter, the emission collected by the cavity corresponds to a
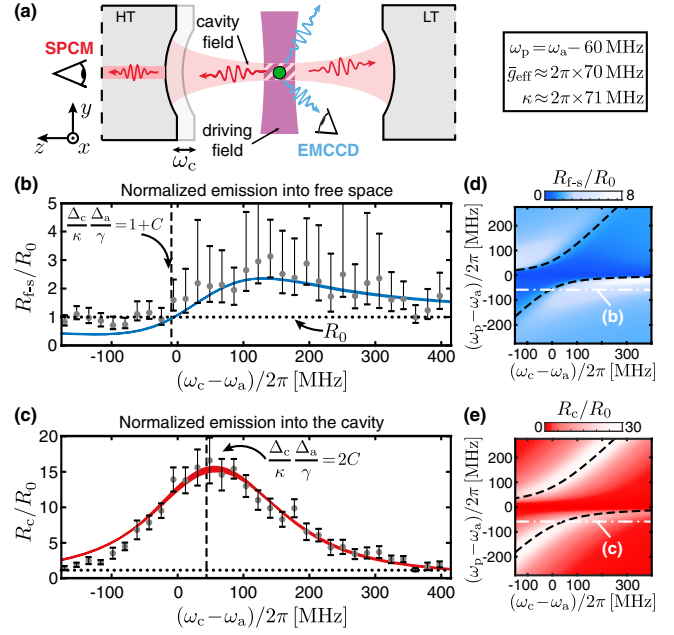

FIG. 3. Cavity backaction on the atomic photoemission rate. (a) Simplified experimental scheme depicting the two (interfering) fields. (b) and (c) display the system's emission in free space and into the cavity respectively, normalized to that of an uncoupled atom (dotted black line). The error bars are extracted from data bootstrapping and Monte Carlo error propagation. The uncertainties in (b) are a consequence of the small free-space collection efficiency and the short trapping lifetimes. The solid lines correspond to the fit to an expanded version of Eqs. (1a) (blue) and (1b) (red) including a convolution for different coupling strengths and optical pumping effects estimated from the master equation simulation (see the Supplemental Material [32]). (d) and (e) show the corresponding full spectra for the normalized emission into both free space and the cavity. The black dashed lines represent the $\Delta_c\Delta_a/(\kappa\gamma) = 1 + C$ region in (d), and the dressed eigenbands $\Delta_c\Delta_a/(\kappa\gamma) = 2C$ in (e).

continuous stream of single photons. The quantum nature of the cavity output is confirmed by performing a Hanbury Brown-Twiss experiment [48], where the field is split in two and detected by independent SPCMs. An antibunching dip is observed in the autocorrelation function $g^{(2)}(\tau)$ of the output for $\tau = 0$, where τ represents the delay time between both detector's readouts (see Fig. 4 and the Supplemental Material [32]). The measurement yields a minimum of
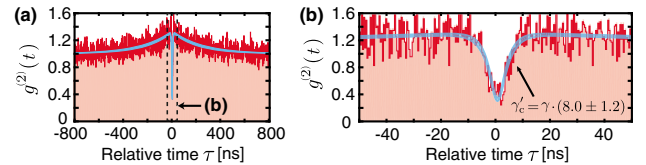

FIG. 4. (a) Autocorrelation function of the cavity output showing the strongly narrowed antibunching dip in (b). The curve is a fit to the phenomenological model described in the Supplemental Material [32].

TABLE I. System's CQED parameters for the different measurements.

Parameter		Fig. 1	Fig. 2	Fig. 3	Fig. 4
Effective coupling	$\bar{g}_{\mathrm{eff}}/2\pi$ [MHz]	50	35	70	40
Cavity linewidth	$\kappa/2\pi$ [MHz]	58	82	71	75
Purcell factor	$f_{\mathrm{P}} = 2\bar{C}$	14.4	5.0	22.6	7.0

$g^{(2)}(0) = (0.34 \pm 0.05) < 0.5$, limited by the detector jitter and consistent with a true single-photon light field. The exponential rise of the dip of $(2\gamma_c')^{-1} = (3.3 \pm 0.5)$ ns is almost an order of magnitude shorter than the natural decay time of the atom $[(2\gamma)^{-1} = 26.24$ ns], thus providing additional evidence of the clear Purcell enhancement in our system, the homogeneous nature of the broadening, and the high repetition rate available when using the platform as an SPS.

In conclusion, we have demonstrated a large Purcell effect in a strongly coupled light-matter platform (see Table I), and we have shown its performance as an efficient and high-bandwidth single-photon interface. A larger trap-induced ac Stark shift would allow us to address the cycling transition through frequency selection of one of the σ components of the external lin⊥lin driving, thus providing a Purcell factor of up to $f_P \approx 190$ (considering a total recovery of the cavity finesse). The resulting cavity collection efficiency (99.5%) would be of central importance for any application with high detection efficiency requirements (e.g., [49]). The high cavity decay rate can also be exploited to bridge the bandwidth mismatch between incoming fast photons (e.g., from quantum dots [50]) and long-lived stationary emitters, like atoms [51]. This is of particular importance for high-bandwidth quantum memories in hybrid links. Extending systems based on atoms in fiber cavities to the more technically relevant telecom wavelengths for quantum repeater applications is possible by using higher-lying atomic levels [52] together with dual-wavelength mirror coatings [53].

*Present address: Wellman Center for Photomedicine, Massachusetts General Hospital and Harvard Medical School, Boston, Massachusetts, 02114, USA. jgallegofernandez@mgh.harvard.edu

[1] E. M. Purcell, Phys. Rev. **69**, 674 (1946).
[2] P. Goy, J. M. Raimond, M. Gross, and S. Haroche, Phys. Rev. Lett. **50**, 1903 (1983).
[3] D. J. Heinzen, J. J. Childs, J. E. Thomas, and M. S. Feld, Phys. Rev. Lett. **58**, 1320 (1987).
[4] Y. H. Lien, G. Barontini, M. Scheucher, M. Mergenthaler, J. Goldwin, and E. A. Hinds, Nat. Commun. **7**, 13933 (2016).
[5] T. G. Ballance, H. M. Meyer, P. Kobel, K. Ott, J. Reichel, and M. Köhl, Phys. Rev. A **95**, 033812 (2017).
[6] J. M. Gérard, B. Sermage, B. Gayral, B. Legrand, E. Costard, and V. Thierry-Mieg, Phys. Rev. Lett. **81**, 1110 (1998).
[7] A. Laucht, T. Günthner, S. Pütz, R. Saive, S. Frédérick, N. Hauke, M. Bichler, M.-C. Amann, A. W. Holleitner, M. Kaniber, and J. J. Finley, J. Appl. Phys. **112**, 093520 (2012).
[8] A. Bienfait, J. J. Pla, Y. Kubo, X. Zhou, M. Stern, C. C. Lo, C. D. Weis, T. Schenkel, D. Vion, D. Esteve, J. J. L. Morton, and P. Bertet, Nature (London) **531**, 74 (2016).
[9] H. Sumikura, E. Kuramochi, H. Taniyama, and M. Notomi, Phys. Rev. B **94**, 195314 (2016).
[10] D. Ding, L. M. C. Pereira, J. F. Bauters, M. J. R. Heck, G. Welker, A. Vantomme, J. E. Bowers, M. J. A. de Dood, and D. Bouwmeester, Nat. Photonics **10**, 385 (2016).
[11] A. Dibos, M. Raha, C. Phenicie, and J. Thompson, Phys. Rev. Lett. **120**, 243601 (2018).
[12] J. McKeever, A. Boca, A. D. Boozer, R. Miller, J. R. Buck, A. Kuzmich, and H. J. Kimble, Science **303**, 1992 (2004).
[13] A. Kuhn, M. Hennrich, and G. Rempe, Phys. Rev. Lett. **89**, 067901 (2002).
[14] D. Press, S. Götzinger, S. Reitzenstein, C. Hofmann, A. Löffler, M. Kamp, A. Forchel, and Y. Yamamoto, Phys. Rev. Lett. **98**, 117402 (2007).
[15] S. Kang, S. Lim, M. Hwang, W. Kim, J.-R. Kim, and K. An, Opt. Express **19**, 2440 (2011).
[16] M. Mücke, J. Bochmann, C. Hahn, A. Neuzner, C. Nölleke, A. Reiserer, G. Rempe, and S. Ritter, Phys. Rev. A **87**, 063805 (2013).
[17] I. Aharonovich, D. Englund, and M. Toth, Nat. Photonics **10**, 631 (2016).
[18] P. R. Dolan, S. Adekanye, A. A. P. Trichet, S. Johnson, L. C. Flatten, Y. C. Chen, L. Weng, D. Hunger, H.-C. Chang, S. Castelletto, and J. M. Smith, Opt. Express **26**, 7056 (2018).
[19] K. J. Vahala, Nature (London) **424**, 839 (2003).
[20] Y. Colombe, T. Steinmetz, G. Dubois, F. Linke, D. Hunger, and J. Reichel, Nature (London) **450**, 272 (2007).
[21] M. Steiner, H. M. Meyer, C. Deutsch, J. Reichel, and M. Köhl, Phys. Rev. Lett. **110**, 043003 (2013).
[22] C. Sayrin, C. Clausen, B. Albrecht, P. Schneeweiss, and A. Rauschenbeutel, Optica **2**, 353 (2015).
[23] S. Kato and T. Aoki, Phys. Rev. Lett. **115**, 093603 (2015).
[24] D. Hunger, T. Steinmetz, Y. Colombe, C. Deutsch, T. W. Hänsch, and J. Reichel, New J. Phys. **12**, 065038 (2010).
[25] H. Kaupp, T. Hümmer, M. Mader, B. Schlederer, J. Benedikter, P. Haeusser, H.-C. Chang, H. Fedder, T. W. Hänsch, and D. Hunger, Phys. Rev. Applied **6**, 054010 (2016).
[26] A. Muller, E. B. Flagg, M. Metcalfe, J. Lawall, and G. S. Solomon, Appl. Phys. Lett. **95**, 173101 (2009).

[27] N. E. Flowers-Jacobs, S. W. Hoch, J. C. Sankey, A. Kashkanova, A. M. Jayich, C. Deutsch, J. Reichel, and J. G. E. Harris, Appl. Phys. Lett. **101,** 221109 (2012).

[28] R. Albrecht, A. Bommer, C. Pauly, F. Mücklich, A. W. Schell, P. Engel, T. Schröder, O. Benson, J. Reichel, and C. Becher, Appl. Phys. Lett. **105,** 073113 (2014).

[29] A. Jeantet, Y. Chassagneux, C. Raynaud, P. Roussignol, J. S. Lauret, B. Besga, J. Estève, J. Reichel, and C. Voisin, Phys. Rev. Lett. **116,** 247402 (2016).

[30] H. Takahashi, E. Kassa, C. Christoforou, and M. Keller, Phys. Rev. A **96,** 023824 (2017).

[31] J. Gallego, S. Ghosh, S. K. Alavi, W. Alt, M. Martinez-Dorantes, D. Meschede, and L. Ratschbacher, Appl. Phys. B: Lasers Opt. **122,** 47 (2016).

[32] See Supplemental Material at http://link.aps.org/supplemental/10.1103/PhysRevLett.121.173603 for a detailed description of relevant experimental techniques and theoretical considerations, which includes Refs. [33–40].

[33] A. Fuhrmanek, R. Bourgain, Y. R. P. Sortais, and A. Browaeys, Phys. Rev. A **85,** 062708 (2012).

[34] S. Kuhr, W. Alt, D. Schrader, I. Dotsenko, Y. Miroshnychenko, A. Rauschenbeutel, and D. Meschede, Phys. Rev. A **72,** 023406 (2005).

[35] K. B. Lee, J. Siegel, S. Webb, S. Lévêque-Fort, M. Cole, R. Jones, K. Dowling, M. Lever, and P. French, Biophys. J. **81,** 1265 (2001).

[36] D. Gangloff, M. Shi, T. Wu, A. Bylinskii, B. Braverman, M. Gutierrez, R. Nichols, J. Li, K. Aichholz, M. Cetina, L. Karpa, B. Jelenković, I. Chuang, and V. Vuletić, Opt. Express **23,** 18014 (2015).

[37] B. Brandstätter, A. McClung, K. Schüppert, B. Casabone, K. Friebe, A. Stute, P. O. Schmidt, C. Deutsch, J. Reichel, R. Blatt, and T. E. Northup, Rev. Sci. Instrum. **84,** 123104 (2013).

[38] S. M. Tan, J. Opt. B **1,** 424 (1999).

[39] E. T. Jaynes and F. W. Cummings, Proc. IEEE **51,** 89 (1963).

[40] S. C. Kitson, P. Jonsson, J. G. Rarity, and P. R. Tapster, Phys. Rev. A **58,** 620 (1998).

[41] M. Martinez-Dorantes, W. Alt, J. Gallego, S. Ghosh, L. Ratschbacher, Y. Völzke, and D. Meschede, Phys. Rev. Lett. **119,** 180503 (2017).

[42] D. Schrader, S. Kuhr, W. Alt, M. Müller, V. Gomer, and D. Meschede, Appl. Phys. B **73,** 819 (2001).

[43] A. V. Gorshkov, A. André, M. D. Lukin, and A. S. Sørensen, Phys. Rev. A **76,** 033804 (2007).

[44] K. Murr, J. Phys. B **36,** 2515 (2003).

[45] P. M. Alsing, D. A. Cardimona, and H. J. Carmichael, Phys. Rev. A **45,** 1793 (1992).

[46] H. Tanji-Suzuki, I. D. Leroux, M. H. Schleier-Smith, M. Cetina, A. Grier, J. Simon, and V. Vuletić, Adv. At. Mol. Opt. Phys. **60,** 201 (2011).

[47] R. Reimann, W. Alt, T. Kampschulte, T. Macha, L. Ratschbacher, N. Thau, S. Yoon, and D. Meschede, Phys. Rev. Lett. **114,** 023601 (2015).

[48] R. H. Brown and R. Q. Twiss, Nature (London) **177,** 27 (1956).

[49] W. Rosenfeld, D. Burchardt, R. Garthoff, K. Redeker, N. Ortegel, M. Rau, and H. Weinfurter, Phys. Rev. Lett. **119,** 010402 (2017).

[50] M. Zopf, T. Macha, R. Keil, E. Uruñuela, Y. Chen, W. Alt, L. Ratschbacher, F. Ding, D. Meschede, and O. G. Schmidt, Phys. Rev. B **98,** 161302(R) (2018).

[51] H. M. Meyer, R. Stockill, M. Steiner, C. Le Gall, C. Matthiesen, E. Clarke, A. Ludwig, J. Reichel, M. Atatüre, and M. Köhl, Phys. Rev. Lett. **114,** 123001 (2015).

[52] M. Uphoff, M. Brekenfeld, G. Rempe, and S. Ritter, Appl. Phys. B **122,** 46 (2016).

[53] S. Garcia, F. Ferri, K. Ott, J. Reichel, and R. Long, Opt. Express **26,** 22249 (2018).

Supplemental Material for "Strong Purcell effect on a neutral atom trapped in an open fiber cavity"

J. Gallego,[*] W. Alt, T. Macha, M. Martinez-Dorantes, D. Pandey, and D. Meschede

Institut für Angewandte Physik der Universität Bonn, Wegelerstrasse 8, D-53115 Bonn, Germany

EXPERIMENTAL METHODS

Finesse degradation

The initial cavity field decay rate of $\kappa = 2\pi \times (24.5 \pm 0.8)\,\text{MHz}$ [S1] increased after the resonator was placed under high-vacuum conditions ($\sim 10^{-9}\,\text{mbar}$), due to a sudden rise of optical losses on the fiber-mirrors' coating. This resulted in a finesse degradation where the type of decay and the time scales involved are strongly influenced by the presence of ultraviolet (UV) light on the mirrors. We observe that UV radiation turned a rapid exponential decay of the finesse into a slower decline with a half-life of ~ 300 days (see Fig. S.1(a)). As a consequence of the finesse variations, the bandwidth of the resonator during the measurements presented in the main text varies between two and three times the initial value. We observe that the finesse can be recovered (up to 80% of the initial value) when flushing the vacuum apparatus with pure oxygen. The recovery process takes place at rates much faster than the ones predicted by the oxygen depletion model [S2, S3]. It remains unclear why UV radiation slows down the degradation process in vacuum, and if it affects both mirrors equally (the surface layer of the mirrors coating is composed of SiO_2 and Ta_2O_5 for the LT and HT mirrors, respectively).

Effective coupling strength

The interaction strength between an atom and the resonator mode varies in our experiments depending on two factors: the transition addressed by the cavity, and the distance of the atom to the center of the Gaussian transversal cavity mode. Regarding the first factor, the strongest coupling is associated to the cycling transition $|F, m_F\rangle = |2, 2\rangle \leftrightarrow |3', 3'\rangle$, corresponding to $g_{\max} = 2\pi \times 120\,\text{MHz}$ for an atom at the center. This is achieved in our experiments when using a circularly-polarized probe laser injected into the cavity. After a few cycles, the light optically pumps the atoms to the outermost Zeeman sublevel of the ground state ($|2, 2\rangle$), thus ensuring the addressing of the strongest transition. The quantization axis is defined by a small bias magnetic field parallel to the resonator and to the electric field of the red-detuned dipole traps. This is not the case when using the lin⊥lin side-probe laser, where the resulting atomic
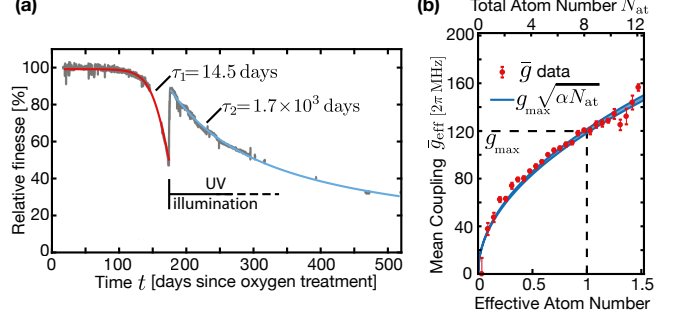

FIG. S.1. (a) Decay of the finesse under vacuum after the first oxygen treatment (monitored with 770 nm light) represented as a percentage of the initial value. The initial decay corresponds to an exponential increase in losses $\mathcal{L}$ of the form $\mathcal{L}(t) = \mathcal{L}_0 + \Delta\mathcal{L} \cdot \exp(t/\tau_1)$ (red curve) yielding a time constant of $\tau_1 = 14.5$ days. With constant UV illumination the finesse quickly recovers (sudden positive slope) and the decay process slows down, following the curve predicted by the oxygen depletion model [S3] given by $\mathcal{L}(t) = \mathcal{L}_0 + \Delta\mathcal{L} \cdot (1 - \exp(-t/\tau_2))$ (blue) with a time constant of $\tau_2 = 1670$ days. (b) Effective coupling of an atomic ensemble for an increasing number of atoms. N_{at} is estimated from fluorescence images of the ensemble. $\alpha = 0.12$ is the reduction factor accounting for imperfect positioning of the atoms.

steady-state population is a mixture of different m_F-sublevels, with the population distribution depending on the frequency of the driving field. For instance, in the cavity backaction measurements, the side probe is red-detuned by 63 MHz from the ac-Stark shifted atomic resonance, to ensure one-dimensional polarization-gradient cooling that extends the trapping lifetime. This detuning and polarization provides on average a population of the outermost m_F sublevels of 40 %, as compared to the 10 % present when pumping at resonance (as the master equation simulations suggest). As a consequence, the atomic excitations do not correspond to the closed cycle and the coupling strength associated to an externally driven atom is effectively reduced to $g_{\text{eff}} < g_{\max}$. The exact reduction factor is extracted from the master equation simulations. A way to address the cycling transition when driving the atom with lin⊥lin light would be to substantially increase the trap depth. The resulting strong ac-Stark shift would lift the degeneracy of the m_F-sublevels of the excited states, thus allowing for frequency selection of the σ_+ component of the light. This would correspond to the cycling transition if the atom has been previously optically pumped to the ground-state $|2, 2\rangle$ sublevel (e.g. by

a cavity-probe pulse).

With respect to the different possible positions of the atom in the cavity mode, the typical loading leads to a distribution of coupling strengths following a Gaussian curve of average $\bar{g}_{\text{eff}} < g_{\text{eff}}$ and of typical width $\sigma_g \approx 2\pi \times 18.2\,\text{MHz}$ when the transport feedback technique is employed. The 2D optical transport capabilities of our system could be used to deterministically place single atoms at the optimum position in the resonator (i.e., by monitoring the cavity reflection while performing a 2D position scan).

When an ensemble (as opposed to a single atom) is coupled to the resonator, we observe that the coupling scales phenomenologically with the number of atoms as

$$\bar{g}_{\text{eff}} \approx \sqrt{0.12 \cdot N_{\text{at}}} \; g_{\text{eff}} \, . \tag{S.1}$$

where the factor 0.12 accounts for the average distance to the cavity center, as shown in Fig. S.1(b). The estimated average coupling from Fig. 1(c) scales slightly more favorable than expected from Eq. S.1, due to the transport feedback scheme pre-selecting atoms at positions of strong coupling. Thus, by coupling dense ensembles instead of single atoms, collective interaction rates could approach the GHz regime. This is critical in hybrid quantum communication links, where the coherent interaction between photonic and stationary qubits must be faster than the cavity decay rate (and ideally higher than the fast-photon bandwidth).

Number of atoms coupled to the cavity (N_{at}): deterministic transport and push-out sequence.

As introduced in the main text, the influence of the atom on the reflective spectrum of the cavity is employed to detect the atom's presence. In particular, when an atom enters the cavity, it shifts its resonance and the cavity-probe beam is reflected leading to a rise in the SPCM counts, which is then used to stop the transport. This signal saturates (i.e., the probe is fully reflected) in the case of strong coupling, meaning that the technique does not distinguish between a single strongly coupled atom or an ensemble of them. In order to ensure that only one atom is coupled to the resonator, we load the conveyor belt sparsely, such that the distance between the few trapped atoms is longer than the transversal cavity mode. The reflection threshold used to stop the transport is typically set at 90% of the maximum of the reflected power. It is worth noting that, independently of the total amount of atoms in the resonator, the number of atoms per trapping site is never bigger than unity. This is due to light-induced collisions [S4] taking place during the trap loading, where the near-resonant MOT beams project the number of atoms per site to either 0 or 1.

By performing fluorescence imaging inside the cavity region after the deterministic transport technique, we observe that less than 15% of the cases lead to the coupling of more than one atom (resulting in an average of $\bar{N}_{\text{at}} = 1.07$ when also considering cases with zero atoms). This sets an upper limit, as the camera also detects fluorescence from atoms close to the cavity mode that are not coupled to it. In the Purcell-broadening measurements we employ the cavity-probe laser as a side probe (since it allowed for a wider frequency scan), and therefore the transport feedback technique is not available. In that case, the average number of atoms is estimated by counting the fraction of traces that have one or more atoms coupled to the cavity (by detecting photons emitted into the resonator), and assuming that the loading process is random and, therefore, Poissonian. We found that 77% of the cases yielded a cavity-output signal over the noise floor (signaling the presence of atoms in the cavity). The 23% of cases with zero atoms leads to a Poissonian distribution with an average of $\bar{N}_{\text{at}} \approx 1.5$.

In the context of the cavity backaction measurements, the signal-to-noise ratio of a coupled-atom's scattering into free space is reduced in the presence of uncoupled atoms in the proximity of the cavity mode, the fluorescence of which is also collected by the high-NA lenses. To avoid such contamination of the fluorescence, we push the atoms that are not coupled to the resonator out of the optical trap. This is done by first using the cavity-probe light to only pump the atom in the resonator into the *dark state* manifold $|F = 1\rangle$ and, subsequently, performing a push-out pulse [S5] with the side-probe beam. This expels all the atoms remaining in the *bright state* $|F = 2\rangle$ out of the trap. The probability of an atom being pumped to the dark state increases with its coupling strength. The technique leads to a preselection of atoms with stronger coupling (manifesting as a rise in the average cooperativity, as shown in the main text), since those that are weakly coupled have a higher chance of remaining in the bright state and being expelled off the trap. As a consequence, the loading in these measurements is expected to be lower than $\bar{N}_{\text{at}} = 1.07$.

Trapping lifetime corrections

Under external laser driving, the atoms continuously scatter photons in all directions resulting in emission recoil events that increase the temperature of the trapped atoms. The polarization gradient of the driving field (side-probe laser) only provides cooling along the illumination axis and, therefore, the atoms accumulate thermal motion in the remaining two directions. This results in trapping losses that hinder the precise estimation of photon emission rates.

Additionally, the loss rate depends on the resonator detuning due to cavity backaction on the total atomic

scattering rate. Such a dependence needs to be characterized, in order to obtain the atom-loss-corrected scattering rates. We average over 150 SPCM data traces for each cavity resonance frequency; from these average traces we infer the atom loss rate from the decay in the counts. Since different coupling strengths lead to different trapping times, the average decay curve is not a single exponential, but a distribution of them. The data is, therefore, fit to a more general *stretched exponential*, defined by $A \cdot \exp[(-t/\tau)^\beta]$. This function represents the time evolution of a system that is driven by a specific distribution of decay processes (given by β), each with a different amplitude A_i and lifetime τ_i [S6]. Although this particular function does not contain a full model of the heating mechanism, we find that such a phenomenological approach is enough for the scattering rate evaluation.

The amplitude A of each averaged trace yields a direct estimation of the output rate of the cavity R_c, as it represents the scattering rate before the heating processes take place. In addition, the decay time of each curve corresponds to the trapping lifetime for the different cavity detunings. The decay behavior is used to estimate the rate $R_{\text{f-s}}$, which is extrapolated from the amount of accumulated photoelectrons n_{ph} on the EMCCD chip during a 100-ms-long exposure. We assume that the free-space emission follows the same decay as the one obtained from the corresponding SCPM traces, and consider $R_{\text{f-s}}$ as the amplitude of the exponential that would lead to n_{ph} photoelectrons when integrating over 100 ms.

Single-photon statistics

In order to characterize the quantum character of the light emitted by the coupled system, we perform a simple experiment – depicted in Fig. S.2 – where we externally drive a single (coupled) atom and collect its emission with the resonator. The photon statistics of the cavity's output field is then analyzed by performing a Hanbury Brown–Twiss experiment [S7] in which the field is split and subsequently detected by two photon counting modules. The cross-correlation between the time-resolved signals of both photodetectors yields the second-order intensity correlation function $g^{(2)}$ of the field

$$g^{(2)}(\tau) = \frac{\langle c_1(t)\, c_2(t+\tau) \rangle}{\langle c_1(t) \rangle \langle c_2(t) \rangle} \, . \qquad \text{(S.2)}$$

Here $c(t)$ is the number of counts detected at time t (either 0 or 1), $\langle \rangle$ is the time average for sufficiently long periods, τ is the delay time between both detection traces, and the subindices 1 and 2 represent the photodetectors.

Effects characteristic of single-photon sources, such as antibunching (corresponding to the absence of two or more photons emitted at the same time), can be directly observed in the $g^{(2)}$ function. In particular, the measured cross-correlation of the cavity output (depicted in
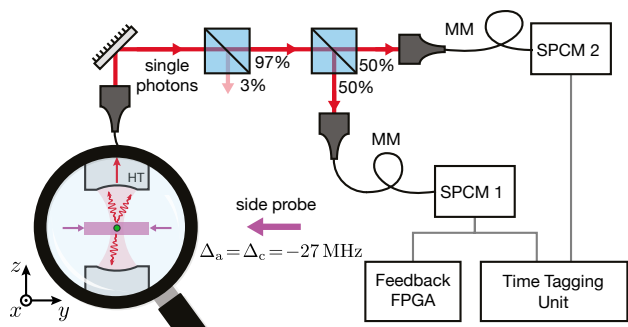

FIG. S.2. Experimental setup for the single-photon generation. A single atom is driven by the side probe (and a repumper field, not shown), and its emission is efficiently collected by the resonator (magnified sketch). The light that leaves through the high-transmission (HT) mirror is guided through the fiber to a 97%/3% beam splitter, used to couple the probe into the cavity during the feedback transport. The single photons are split and sent to both multi-mode (MM-) fiber-inputs of the detectors (SPCM 1,2), the output of which is registered in a time tagging unit (81 ps resolution). The signal from SPCM 1 is duplicated and sent to an FPGA card that computes and generates the signal to stop the optical transport.

Fig. 4 in the main text) shows both an antibunching dip at $\tau = 0$, followed by a bunching feature ($g^{(2)} > 1$) around the central dip. While the dip manifests the quantum nature of the field, the bunching behavior is attributed to insufficient optical power of the repumper field which causes the atom to spend a considerable fraction of the time in the dark state. The typical emission pattern is thus comprised of emission windows separated by "dark" periods, and the compression or "clustering" of photons in packets leads to the bunching. The behavior can be described phenomenologically by a simple model given by (see e.g. [S8])

$$g^{(2)}(\tau) = 1 - (1+b)e^{-2\tau\gamma_c'} + be^{-\tau/\tau_b} \, , \qquad \text{(S.3)}$$

where b and τ_b describe the amplitude and decay time that characterize the photon bunching, and $(2\gamma_c')^{-1}$ stands for the enhanced atomic decay rate.

In this case $(2\gamma_c')^{-1} = (3.3 \pm 0.5)$ ns, which is to be compared to the natural decay time of $(2\gamma)^{-1} = 26.24$ ns. We account for the limited time resolution of the detectors by convolving Eq. S.3 with a Gaussian of width $\sigma = 1.35$ ns, which describes the specified detectors' jittering. The fast atomic decay and the considerable bunching amplitude ($b = 0.33$) reduce the effective width of the antibunching dip. In combination with the detectors jittering, the feature is washed out and the central value of the fit model rises, leading in our case to the value $g^{(2)}(0) = 0.34 \pm 0.05$.

THEORETICAL CONSIDERATIONS

The driven, dissipative system

In the absence of dissipative channels, the closed atom–cavity system is fully described by the Jaynes–Cummings Hamiltonian [S9] which, under the rotating wave approximation, is given by

$$\hat{H}_{\mathrm{JC}} = \hbar\omega_{\mathrm{a}}\,\hat{\sigma}^{\dagger}\hat{\sigma} + \hbar\omega_{\mathrm{c}}\,\hat{a}^{\dagger}\hat{a} + \hbar g\left(\hat{\sigma}^{\dagger}\hat{a} + \hat{\sigma}\,\hat{a}^{\dagger}\right), \quad (\mathrm{S.4})$$

where $\hbar$ is Plank's constant and $\hat{\sigma}$ and $\hat{a}$ are the atomic lowering and the photon annihilation operators respectively. This simple description is enough to characterize the energy bands of a single excitation in the coupled system (shown in Fig. 1(c) in the main text). However it does not contain the external-driving term necessary to explore the Purcell and backaction dynamics, which lie at the heart of the experiments presented here.

We consider the atom as a two-level system and that the external driving ($\propto \Omega$) is weak enough to create maximum one excitation. The open, driven system can then be heuristically described by a non-Hermitian Hamiltonian (see e.g. [S10])

$$\hat{H}_{\Omega} = \hat{H}_{\mathrm{JC}} - i\hbar(\gamma\hat{\sigma}^{\dagger}\hat{\sigma} + \kappa\hat{a}^{\dagger}\hat{a}) + \frac{\Omega}{2}\left(\hat{\sigma}^{\dagger} + \hat{\sigma}\right) \quad (\mathrm{S.5})$$

that includes the irreversible dissipative losses (imaginary term) and the external weak pumping (last term). Employing Heisenberg's equation on both cavity and atomic amplitude operators ($\hat{a}^{\dagger}\hat{a}$ and $\hat{\sigma}^{\dagger}\hat{\sigma}$) – and assuming a steady state scenario – provides the scattering rate of photons emitted into the cavity and in free space, respectively:

$$R_{\text{f-s}} = 2\gamma\langle\hat{\sigma}^{\dagger}\hat{\sigma}\rangle_s \quad (\mathrm{S.6a})$$

$$R_{\mathrm{c}} = 2\kappa\langle\hat{a}^{\dagger}\hat{a}\rangle_s, \quad (\mathrm{S.6b})$$

which leads to Eqs. 1(a,b) in the main text. Notice that R_{c} here represents the amount of photons leaving the cavity, of which a fraction $\eta_{\mathrm{HT}} = 67\,\%$ (for the initial finesse) is collected through the HT-fiber output. Considering the optical path losses and the SPCM quantum efficiency, only $\eta_{\mathrm{c}} \approx 2.1\,\%$ of the cavity output rate R_{c} is finally detected in the cavity backaction measurements (where the finesse decay reduced η_{HT} to $18\,\%$).

Master equation corrections

The external side-driving of the atom in our measurements is constituted by a lin⊥lin polarization gradient that effectively drives both π- and $\sigma_{\pm}$-transitions between the $|F=2\rangle \to |F'=3\rangle$ sublevels (if averaging over several atom positions). As a consequence, the atom cannot be considered a two-level system any longer. Furthermore, in some cases the driving powers employed are of the order of the saturation intensity, and the weak excitation approximation does not hold.

To describe the system in such scenario we resort to the master equation (ME) formalism, where the system of interest (described by a reduced density matrix) evolves according to a Liouvillian operator containing the environmental degrees of freedom. Although analytical solutions of the ME are not available for this level of complexity, there are numerical computational approaches [S11] that provide steady-state solutions. The numerical results are used to benchmark the simplified model. Indeed, we observe that the simulations qualitatively confirm the system's behavior predicted from Eqs. 1, except for small correction factors on the systems main parameters – namely the coupling strength, the cavity bandwidth, the detunings, and the photon collection efficiencies. We simulate the measurement conditions and obtain correction factors for said parameters by comparing both methods. For example, when simulating the red-detuned illumination used in the cavity backaction measurements, we observe that the numerically calculated scattering rates closely follow the behavior from Eqs. 1, as long as one accounts for a reduction of 5% in g and a rise of 15% in κ. These effects are then included in the fitting model (except for g, which is used as a free parameter anyway).

Cavity backaction fit

The fit shown in Fig. 3 (main text) is part of a single fit commonly applied to four of such pair of curves, which corresponds to the same type of measurement with different driving laser powers (see Fig. S.3). The fit assumes a single free-space collection efficiency $\eta_{\text{f-s}}$ for all measurements, as well as the same resonator bandwidth κ and an unknown frequency offset of the cavity resonance ω_{c}. Without such frequency offset, we observe an obvious systematic discrepancy between the eight data sets and the common fit. The discrepancy is considerably reduced when assuming the cavity resonance frequency as a free parameter, while the extracted cooperativity only varies by 15 %. The exact origin of the 70 MHz shift is unclear, but we attribute it to thermal (or heating) effects on the atoms, which are not included in our simulations. This influences the atomic emission properties, e.g. different effective ac-Stark shifts for different atom's temperatures. Additionally, each measurement pair has the coupling strength as a free parameter (four in total), since higher driving powers induce more heating and therefore smaller effective coupling constants. This leads to seven free parameters for eight curves.
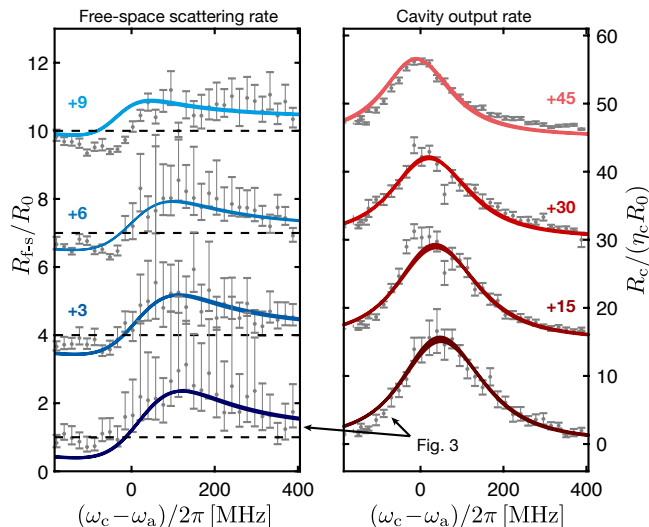
FIG. S.3. Free-space (blue, left) and cavity (red, right) emission rates from a single atom for different cavity resonance frequencies (horizontal axes). Each plot contains four data sets corresponding to different illumination powers (6.5 mW, 25 mW, 65 mW and 250 mW from bottom to top), which are vertically shifted for better clarity. The curves correspond to a single fit to our model (see discussion and Fig. 3 in the main text). The dashed, black lines correspond to R_0.

The cavity collection efficiency η_c was determined in an independent calibration to be $\sim 2.1\%$. A direct measurement of the free-space detection efficiency $\eta_{\text{f-s}}$, though, remains challenging. The collection capability of the high-NA lens depends on the dipole emission pattern of the atom, which varies for different cavity resonant frequencies due to optical pumping effects. An approximation considering the emission dipole of an atom driven with lin⊥lin light (and no cavity present) yields $\eta_{\text{f-s}} = 2.2\%$, in contrast to the value retrieved from the fit of $\eta'_{\text{f-s}} = 3.3 \pm 0.1\%$.

The effective cooperativity extracted from the fits differs for the free-space and cavity emission curves. Al-

though both (cavity and free-space emission) curves are extracted from the same measurement (and therefore same average atomic coupling), the master equation simulation predicts that optical pumping effects lead to a behavior equivalent to reductions on g of 5 % for R_c and 11 % for $R_{\text{f-s}}$. In combination with the fit parameters, this results in effective average cooperativities of $\bar{C}_{1,c} = 12.6 \pm 0.8$ and $\bar{C}_{1,\text{f-s}} = 10.0 \pm 0.6$, respectively (their arithmetic mean is the value reported in the main text).

* gallego@iap.uni-bonn.de
[S1] J. Gallego, S. Ghosh, S. K. Alavi, W. Alt, M. Martinez-Dorantes, D. Meschede, and L. Ratschbacher, Applied Physics B: Lasers and Optics 122, 47 (2016).
[S2] B. Brandstätter, A. McClung, K. Schüppert, B. Casabone, K. Friebe, A. Stute, P. O. Schmidt, C. Deutsch, J. Reichel, R. Blatt, and T. E. Northup, Review of Scientific Instruments 84, 123104 (2013).
[S3] D. Gangloff, M. Shi, T. Wu, A. Bylinskii, B. Braverman, M. Gutierrez, R. Nichols, J. Li, K. Aichholz, M. Cetina, L. Karpa, B. Jelenković, I. Chuang, and V. Vuletić, Opt. Express 23, 18014 (2015).
[S4] A. Fuhrmanek, R. Bourgain, Y. R. P. Sortais, and A. Browaeys, Phys. Rev. A 85, 062708 (2012).
[S5] S. Kuhr, W. Alt, D. Schrader, I. Dotsenko, Y. Miroshnychenko, A. Rauschenbeutel, and D. Meschede, Phys. Rev. A 72, 023406 (2005).
[S6] K. B. Lee, J. Siegel, S. Webb, S. Lévêque-Fort, M. Cole, R. Jones, K. Dowling, M. Lever, and P. French, Biophysical Journal 81, 1265 (2001).
[S7] R. H. Brown and R. Q. Twiss, Nature 177, 27 (1956).
[S8] S. C. Kitson, P. Jonsson, J. G. Rarity, and P. R. Tapster, Phys. Rev. A 58, 620 (1998).
[S9] E. T. Jaynes and F. W. Cummings, Proceedings of the IEEE 51, 89 (1963).
[S10] Y. H. Lien, G. Barontini, M. Scheucher, M. Mergenthaler, J. Goldwin, and E. A. Hinds, Nature Communications 7, 13933 (2016).
[S11] S. M. Tan, J. Opt. B: Quantum Semiclass. Opt 1, 424 (1999).